Journal of Sound and Vibration 329 (2010) 2068–2082

Contents lists available at ScienceDirect

Journal of Sound and Vibration

journal homepage: www.elsevier.com/locate/jsvi

Design of shaped piezoelectric modal sensor for beam with arbitrary boundary conditions by using Adomian decomposition method

Qibo Mao *, Stanislaw Pietrzko

Empa, Swiss Federal Laboratories for Materials Testing and Research, Ueberlandstrasse 129, CH-8600 Duebendorf, Switzerland

ARTICLE INFO

Article history:
Received 9 February 2009
Received in revised form
6 October 2009
Accepted 13 December 2009
Handling Editor H. Ouyang
Available online 6 January 2010

ABSTRACT

The theory for designing distributed piezoelectric modal sensors is well established for beam structures. However, the current modal sensor theory is limited in scope in that it can only be applied in the case of classical boundary conditions (i.e., either clamped, free, simply supported or sliding). In this paper a solution to the problem of finding the shape of piezoelectric modal sensors for a beam with arbitrary boundary conditions is proposed, using the Adomian decomposition method (ADM). A general expression for designing the shape of a piezoelectric modal sensor is presented, in which the output signal of the designed sensor is proportional to the response of the target mode. Other modes are filtered out. The modal sensor shape is expressed as a function of the second spatial derivative of the structural mode shape function. Based on the ADM and employing some simple mathematical operations, the closed-form series solution of the second spatial derivative of the mode shapes can be determined. Then the shapes of the designed modal sensors are obtained. Finally, some numerical examples are given to demonstrate the feasibility of the proposed modal sensors. It is shown that, for classical boundary conditions, the shapes of the modal sensors based on the ADM agree well with analytical and numerical results given in the literature. For general boundary conditions it is found that the shape of the modal sensors is influenced by the number of modes of interest because the second spatial derivatives of the mode shapes are not orthogonal to one another. The modal sensors for general boundary conditions can be considered as modal filters within a limited frequency band.

1. Introduction

For many years research has been conducted on the design and implementation of shaped piezoelectric modal sensors [1,2] as applied to active vibration control (AVC) and active structural acoustic control (ASAC). In general, shaped piezoelectric sensors made of polyvinylidene fluoride (PVDF) are chosen since these add little loading to light structures and in addition are easy to cut into desired shapes. The design of modal sensors using shaped PVDF film can be traced back to Lee and Moon [1]. The PVDF sensors are designed by shaping the surface electrode, whereby the output of the sensor can be made sensitive to selected modal coordinates, other modal coordinates may be filtered out. Modal sensors measure either a targeted structural mode [1–8] for AVC or the volume velocity/displacement [9–20] for ASAC. Using modal sensors in active control reduces spillover, where high-frequency unmodelled modes would influence the stability of the closed-loop system.

* Corresponding author. Tel.: +41 44 823 4527; fax: +41 44 823 4793.
E-mail address: qibo.mao@empa.ch (Q. Mao).

0022-460X/$ - see front matter © 2009 Elsevier Ltd. All rights reserved.
doi:10.1016/j.jsv.2009.12.016

A modal sensor for a beam-type structure can be obtained by varying the sensor width along the length of the beam. If the sensor covers the entire beam the shape of the sensor may be derived using the mode shape orthogonality property. In this regard, Lee and Moon [1] have shown for the case of a uniform bending beam with classical boundary conditions that the functions defined by the surface strains associated with each mode shape form an orthogonal set. As a result, it is possible to design the shape of the modal sensor by simply assigning a shape function proportional to the second spatial derivative of the mode shape of interest. Tanaka et al. [2,3,11] discussed shaped PVDF sensors for estimating the radiation modes or the particular structural mode of interest from a simply supported plate. Gawronski [4] considered the case of discrete sensors and actuators, and from these derived continuous actuator widths. Anthony [5] performed theoretical and experimental studies involving the design of PVDF modal sensors for a simply supported non-uniform thickness beam. Donoso and Bellido [6] proposed a new way to systematically design distributed piezoelectric modal sensors for circular plates with polar symmetric boundary conditions based on a linear optimization approach. Preumont et al. [17,18] studied spatial filtering using distributed PVDF films.

Until now, most of the applications of shaped piezoelectric modal sensor have been limited to those involving beams and plates with classical boundary conditions (i.e., which are either clamped, free, simply supported or sliding). In practice however, the characteristics of a test structure may very well depart from these classical boundary conditions. Therefore, a method to design a modal sensor for a bending beam of general boundary conditions has yet to be developed. Recently, Friswell and Jiana [21,22] presented an optimization approach to design distributed modal sensors for beam and plate structures based on the finite element method for general boundary conditions.

In this paper, a new computed approach called the Adomian decomposition method [23–29] is introduced to design the shapes of piezoelectric modal sensors for beams with arbitrary boundary conditions. The Adomian decomposition method (ADM) is a useful and powerful method for solving linear and nonlinear differential equations. The goal of ADM is to find the solution of linear and nonlinear, ordinary or partial differential equations without depending on any small parameter such as the case with the perturbation method. In this method the solution is considered as a sum of an infinite series, and rapidly convergence to an accurate solution [24,25]. In recent years, it has been applied to the problem of vibration of structural and mechanical systems [26–29].

Using ADM, the governing differential equation becomes a recursive algebraic equation and boundary conditions become simple algebraic frequency equations which are suitable for symbolic computation [27,28]. Moreover, after some simple algebraic operations on these frequency equations, we can obtain the closed-form series solution of mode shape and the second spatial derivative of the mode shape simultaneously.

A general expression for designing the shape of piezoelectric modal sensor is then presented, in which the output signal of the designed sensor can measure the selected structural mode and filter out the responses of the other modes. Finally, some numerical examples are given to demonstrate the feasibility of the proposed modal sensors.

2. Design of the modal sensors using shaped PVDF sensors

Consider a beam with length L_x, width b and thickness h. A shaped PVDF film of constant thickness is attached onto the top surface and spanned across the entire length of the beam, as shown in Fig. 1. The charge density D_3 of the PVDF sensor can be determined by using the follow constitutive equation [1]:

$$D_3 = e_{31}S_1 + \varepsilon_{33}^S E_3 \tag{1}$$

where S_1 is the bending strain, ε_{33}^S the permittivity at constant strain, E_3 is electric field and e_{31} is the charge density per unit strain in the x-direction.

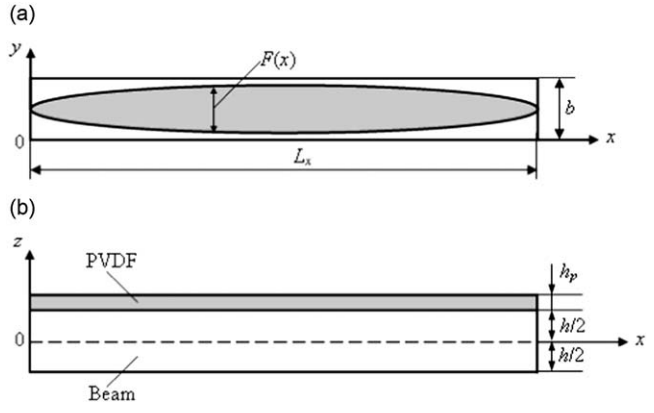

Fig. 1. A shaped PVDF film bonded on a beam: (a) top view and (b) front view.

Assume that the electrodes of the PVDF film are connected to a charge amplifier, the electric field E_3 across the piezoelectric film will be cancelled [17], that is $E_3 = 0$ and $D_3 = e_{31}S_1$. As referred to Lee and Moon's work [1], the output charge $Q(t)$ of the PVDF sensor shown in Fig. 1 can be expressed as

$$Q(t) = \int_0^{L_x} F(x) \cdot D_3(x,t)\,\mathrm{d}x = \int_0^{L_x} F(x) \cdot e_{31}S_1(x,t)\,\mathrm{d}x = \frac{h+h_p}{2}\int_0^{L_x} F(x) \cdot \left(e_{31}\frac{\partial^2 w(x,t)}{\partial x^2}\right)\mathrm{d}x \tag{2}$$

where

$$S_1(x,t) = \frac{h+h_p}{2}\,\frac{\partial^2 w(x,t)}{\partial x^2},$$

h and h_p are the beam and PVDF sensor thickness, respectively. $w(x, t)$ is the displacement of the beam and $F(x)$ is the PVDF film shape function.

The displacement distribution of the vibrating beam may be represented by a series expansion:

$$w(x,t) = \sum_{n=1}^{N} \eta_n(t)\phi_n(x) \tag{3}$$

where $\eta_n(t)$ and $\phi_n(x)$ are the nth modal coordinates and structural mode shape function. N is the index for the highest order structural mode.

Substituting Eq. (3) into (2), and expressing in dimensionless form, one obtains:

$$Q(t) = \frac{h+h_p}{2L_x}e_{31}\sum_{n=1}^{N}\eta_n(t)\int_0^1 F(X)\cdot\frac{\partial^2\Phi_n(X)}{\partial x^2}\,\mathrm{d}X = S\sum_{n=1}^{N}\eta_n(t)P_n \tag{4}$$

where $X = x/L_x$, $\Phi_n(X) = \phi_n(x)$,

$$S = \frac{h+h_p}{2L_x}e_{31}, \quad P_n = \int_0^1 F(X)\cdot\frac{\partial^2\Phi_n(X)}{\partial x^2}\,\mathrm{d}X,$$

is designated as the modal sensitivity [8,22].

To construct a sensor that accurately measures the target structural mode, a shaped PVDF film is used, the output signal of the sensor should be directly proportional to the target modal information. To design the appropriate PVDF film shape function $F(X)$, we make an approximation by expanding $F(X)$ as a function of the second derivative of the basis function of the vibrating beam.

$$F(X) = \sum_{j=1}^{N} B_j\frac{\partial^2\Phi_j(X)}{\partial X^2} \tag{5}$$

where B_j are the unknown shape coefficients for the PVDF sensor.

Substituting Eq. (5) into (4), we obtain:

$$Q(t) = S\sum_{n=1}^{N}\sum_{j=1}^{N}B_k\int_0^1\frac{\partial^2\Phi_n(X)}{\partial X^2}\cdot\frac{\partial^2\Phi_j(X)}{\partial X^2}\,\mathrm{d}X\cdot\eta_n(t) \tag{6}$$

Eq. (6) can be simplified as a matrix form:

$$Q(t) = S\boldsymbol{B}^{\mathrm{T}}\boldsymbol{K}\boldsymbol{\eta} \tag{7}$$

where $\boldsymbol{B}$ and $\boldsymbol{\eta}$ are the $N\times 1$ vectors. $\boldsymbol{K}$ is an $N\times N$ matrix with element:

$$K(n,j) = \int_0^1\frac{\partial^2\Phi_n(X)}{\partial X^2}\cdot\frac{\partial^2\Phi_j(X)}{\partial X^2}\,\mathrm{d}X \tag{8}$$

To design a modal sensor for the Jth structural mode which only measures the target Jth structural mode, and is orthogonal to other modes, for simplicity, we set modal sensitivity P_n in Eq. (4) to

$$P_n = \begin{cases} 1 & n = J \\ 0 & n \neq J \end{cases} \quad \text{for } n = 1,\ldots,N \tag{9}$$

Comparing Eq. (7) and (4) yields:

$$Q(t) = S\boldsymbol{B}^{\mathrm{T}}\boldsymbol{K}\boldsymbol{\eta} = S\boldsymbol{P}^{\mathrm{T}}\boldsymbol{\eta} \tag{10}$$

where $\boldsymbol{P}$ is an $N\times 1$ vector with each element defined in Eq. (9).

From Eqs. (9) and (10), the PVDF sensor shape coefficient vector $\boldsymbol{B}$ can be solved by

$$\boldsymbol{B}^{\mathrm{T}} = \boldsymbol{P}^{\mathrm{T}}\boldsymbol{K}^{-1} = \sum_{j=1}^{N}K^{-1}(j,J) \tag{11}$$

For a beam with classical boundary conditions (such as clamped, free, simply supported or sliding), thanks to the orthogonality of the mode shapes, it is simple to show that $\boldsymbol{K}$ is a diagonal matrix and

$$K^{-1}(j,J)=0 \quad j\neq J \tag{12}$$

Thus, the modal sensor shape coefficients B_k for the classical boundary conditions can be simplified to

$$B_j=\begin{cases}\dfrac{1}{K_{JJ}} & j=J,\\ 0 & j\neq J,\end{cases} \quad F(x)=\frac{1}{K_{JJ}}\frac{\partial^2\Phi_J(x)}{\partial x^2} \tag{13}$$

From Eq. (13), it is shown that the shape of the modal sensor is proportional to the second spatial derivative of the mode shape of interest. It should be noted again that Eq. (13) is only valid for a beam with classical boundary conditions. Eq. (13) can be regarded as a special case of Eq. (11). For a beam with general boundary conditions the orthogonality of the second spatial derivative of the mode shapes cannot be satisfied.

In accordance with the above analysis, to design a modal sensor, the second spatial derivative of the mode shapes must be obtained. This is discussed in the next section by using ADM technique.

3. Calculation of the second spatial derivative of mode shape by using the ADM

Assuming that the PVDF sensor thickness h_p is much smaller than beam thickness h, the mass and stiffness of the sensor is then negligible compared to the properties of the beam. This is a reasonable assumption since the sensor thickness is typically 28–110 μm. The beam with shaped PVDF sensor shown in Fig. 1 can then be considered as a uniform beam (PVDF mass and stiffness effect neglected). Assume the beam is elastically restrained at both ends, as shown in Fig. 2. The partial differential equation describing the free vibration is as follows [27]:

$$\frac{\partial^4 w(x,t)}{\partial x^4}+\frac{m}{EI}\frac{\partial^2 w(x,t)}{\partial t^2}=0 \tag{14}$$

where E is Young's modulus, I is the cross-sectional moment of inertia of the beam $I=bh^3/12$, EI is the bending stiffness. $m=\rho bh$ is the mass per unit length and ρ is the density of the beam.

According to the modal analysis approach (for harmonic free vibration), the $w(x,t)$ can be separated in space and time:

$$w(x,t)=\phi(x)e^{i\omega t} \tag{15}$$

where $\phi(x)$ and ω are the structural mode shape function and the natural frequency, respectively. $i=\sqrt{-1}$.

Substituting Eq. (15) in (14) and separating the variables for time t and space x, the ordinary differential equation is obtained:

$$\frac{d^4\phi(x)}{dx^4}-\frac{m\omega^2}{EI}\phi(x)=0 \tag{16}$$

The boundary conditions at the ends of the beam shown in Fig. 2 can be expressed as

$$EI\frac{d^2\phi(x)}{dx^2}-k_{L1}\frac{d\phi(x)}{dx}=0, \quad EI\frac{d^3\phi(x)}{dx^3}+k_{L0}\phi(x)=0 \ \text{ at } x=0 \tag{17}$$

$$EI\frac{d^2\phi(x)}{dx^2}+k_{R1}\frac{d\phi(x)}{dx}=0, \quad EI\frac{d^3\phi(x)}{dx^3}-k_{R2}\phi(x)=0 \ \text{ at } x=L_x \tag{18}$$

where k_{L0} and k_{R0} are the stiffness of the translational springs, and k_{L1} and k_{R1} are the stiffness of the rotational springs at x=0 and L_x, respectively.

Eq. (16) can be rewritten in dimensionless form:

$$\frac{d^4\Phi(X)}{dX^4}-k\Phi(X)=0 \tag{19}$$

where $X=x/L_x$, $\Phi(X)=\phi(x)$, $k=m\omega^2L_x^4/EI$ is the dimensionless natural frequency parameter.

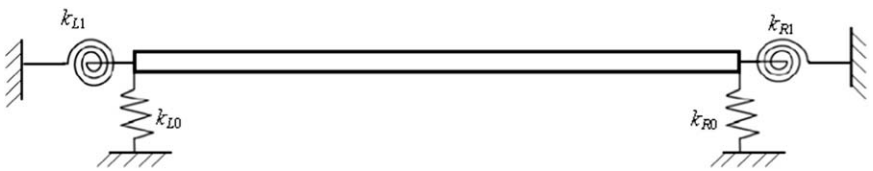

Fig. 2. A uniform beam elastically restrained at both ends.

According to ADM [23–28], $\Phi(X)$ in Eq. (19) can be expressed in terms of an infinite series:

$$\Phi(X) = \sum_{m=0}^{\infty} \Phi^{[m]}(X) \tag{20}$$

where the component function $\Phi^{[m]}(X)$ will be determined recurrently.

Imposing a linear operator $L = \mathrm{d}^4/\mathrm{d}X^4$, the inverse operator of L is then a 4-fold integral operator defined by

$$L^{-1} = \int\int\int\int (\ldots)\,\mathrm{d}X\,\mathrm{d}X\,\mathrm{d}X\,\mathrm{d}X \tag{21}$$

and

$$L^{-1}L(\Phi(X)) = \Phi(X) - \Phi(0) - \frac{\mathrm{d}\Phi(0)}{\mathrm{d}X}X - \frac{\mathrm{d}^2\Phi(0)}{\mathrm{d}X^2}\frac{X^2}{2} - \frac{\mathrm{d}^3\Phi(0)}{\mathrm{d}X^3}\frac{X^3}{6} \tag{22}$$

Applying L^{-1} on both sides of Eq. (19), we obtain:

$$L^{-1}L(\Phi(X)) = kL^{-1}(\Phi(X)) = kL^{-1}\Big(\sum_{m=0}^{\infty} \Phi^{[m]}(X)\Big) \tag{23}$$

Comparing Eqs. (23) and (22), we obtain:

$$\Phi(X) = \Phi(0) + \frac{\mathrm{d}\Phi(0)}{\mathrm{d}X}X + \frac{\mathrm{d}^2\Phi(0)}{\mathrm{d}X^2}\frac{X^2}{2} + \frac{\mathrm{d}^3\Phi(0)}{\mathrm{d}X^3}\frac{X^3}{6} + kL^{-1}\Big(\sum_{m=0}^{\infty} \Phi^{[m]}(X)\Big) \tag{24}$$

Table 1
Values of the stiffness of the translational and the rotational springs for several classical boundary conditions.

	K_{L0}	K_{L1}	K_{R0}	K_{R1}
Clamped-free	10^9	10^9	0	0
Simply supported	10^9	0	10^9	0
Clamped–clamped	10^9	10^9	10^9	10^9

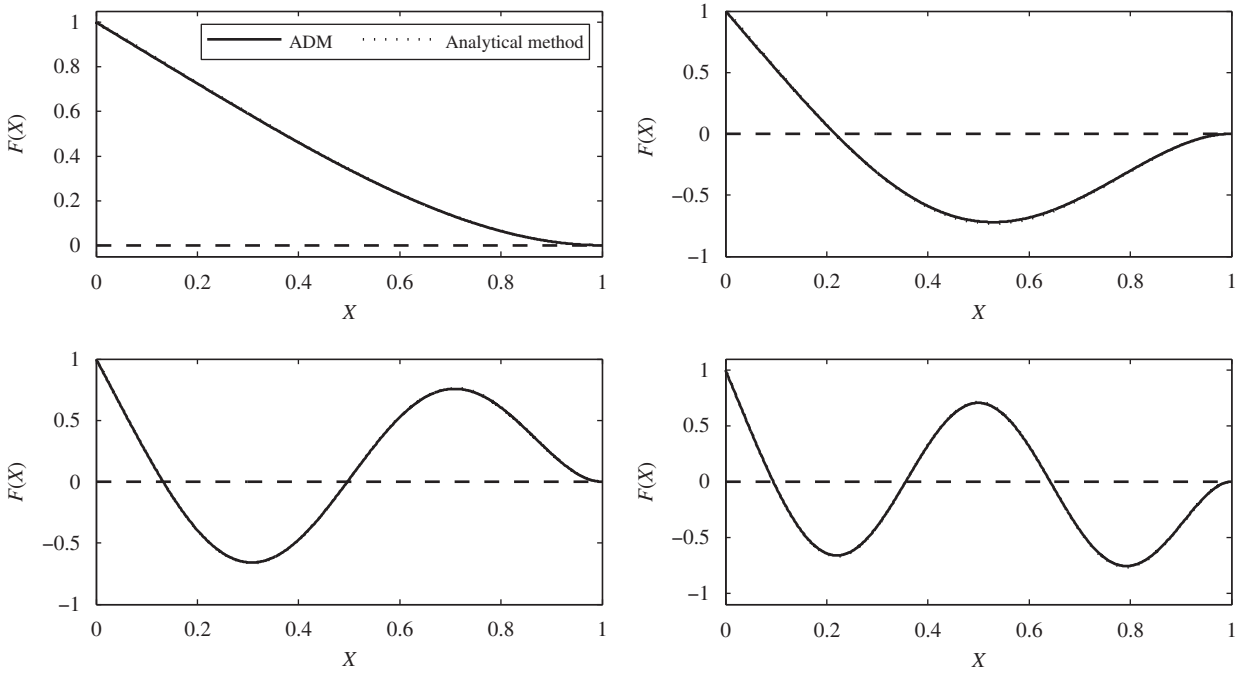

Fig. 3. The modal sensor shapes of the first four modes for the clamped-free beam.

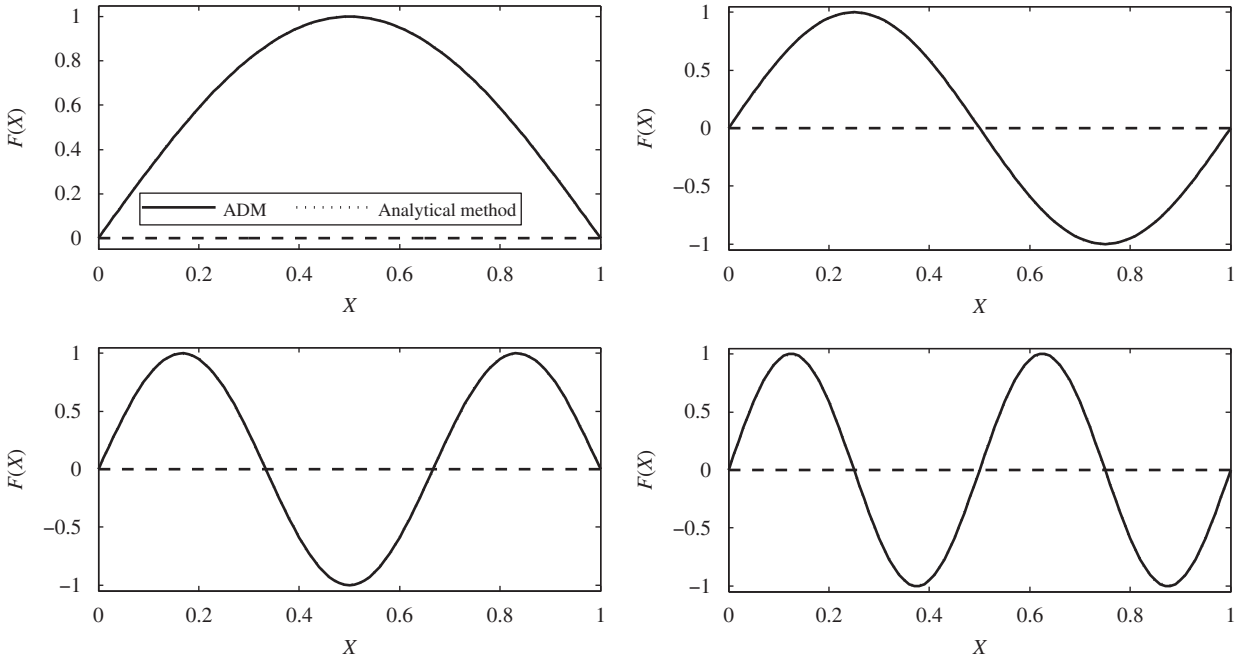

Fig. 4. The modal sensor shapes of the first four modes for the simply supported beam.

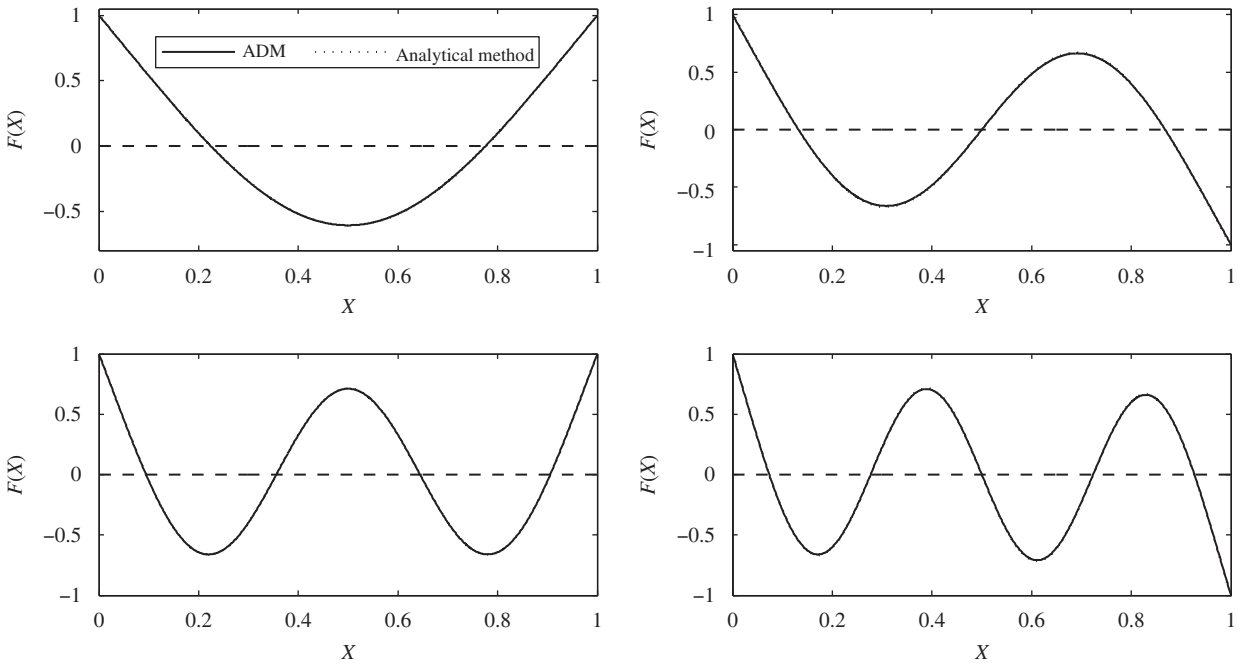

Fig. 5. The modal sensor shapes of the first four modes for the clamped–clamped beam.

Table 2
Two cases illustrating the design of modal sensors.

Boundary conditions	Case A	Case B
At left end ($X=0$)	$K_{R0}=10^9$, $K_{R1}=10^9$	$K_{L0}=10^9$, $K_{L1}=10$
At right end ($X=1$)	$K_{R0}=10$, $K_{R1}=10$	$K_{R0}=10^9$, $K_{R1}=10$

According to standard Adomian decomposition method (see Appendix A), the approximate solution of Eq. (24) is determined by using the following recurrence relation:

$$\Phi^{[0]}(X) = \Phi(0) + \frac{\mathrm{d}\Phi(0)}{\mathrm{d}X}X + \frac{\mathrm{d}^2\Phi(0)}{\mathrm{d}X^2}\frac{X^2}{2} + \frac{\mathrm{d}^3\Phi(0)}{\mathrm{d}X^3}\frac{X^3}{6} \tag{25a}$$

$$\Phi^{[m]}(X) = kL^{-1}(\Phi^{[m-1]}(X)) \quad m \geq 1 \tag{25b}$$

We may approximate the above solution by the truncated series:

$$\Phi(X) = \sum_{m=0}^{M-1} \Phi^{[m]}(X) = \sum_{j=0}^{3} \frac{\mathrm{d}^j\Phi(0)}{\mathrm{d}X^j} \sum_{m=0}^{M-1} \left[k^m \frac{X^{4m+j}}{(4m+j)!} \right] \tag{26}$$

Eq. (26) implies that $\sum_{m=M}^{\infty} \Phi^{[m]}(X)$ is negligibly small. The number of terms M is determined by convergence requirement in practice.

According to Eq. (26), the first, second and third spatial derivative of the mode shapes can be expressed as

$$\frac{\mathrm{d}\Phi(X)}{\mathrm{d}X} = \Phi(0) \sum_{m=1}^{M-1} \left[k^m \frac{X^{4m-1}}{(4m-1)!} \right] + \sum_{j=1}^{3} \frac{\mathrm{d}^j\Phi(0)}{\mathrm{d}X^j} \sum_{m=0}^{M-1} \left[k^m \frac{X^{4m+j-1}}{(4m+j-1)!} \right] \tag{27}$$

$$\frac{\mathrm{d}^2\Phi(X)}{\mathrm{d}X^2} = \sum_{j=0}^{1} \frac{\mathrm{d}^j\Phi(0)}{\mathrm{d}X^j} \sum_{m=1}^{M-1} \left[k^m \frac{X^{4m+j-2}}{(4m+j-2)!} \right] + \sum_{j=2}^{3} \frac{\mathrm{d}^j\Phi(0)}{\mathrm{d}X^j} \sum_{m=0}^{M-1} \left[k^m \frac{X^{4m+j-2}}{(4m+j-2)!} \right] \tag{28}$$

$$\frac{\mathrm{d}^3\Phi(X)}{\mathrm{d}X^3} = \sum_{j=0}^{2} \frac{\mathrm{d}^j\Phi(0)}{\mathrm{d}X^j} \sum_{m=1}^{M-1} \left[k^m \frac{X^{4m+j-3}}{(4m+j-3)!} \right] + \frac{\mathrm{d}^3\Phi(0)}{\mathrm{d}X^3} \sum_{m=0}^{M-1} \left[k^m \frac{X^{4m}}{(4m)!} \right] \tag{29}$$

To calculate $\mathrm{d}^2\Phi(X)/\mathrm{d}X^2$ in Eq. (28), it can be shown there are five unknown parameters, namely $\mathrm{d}^n\Phi(0)/\mathrm{d}X^n$ (n=0, 1, 2, 3) and k, to be determined. These parameters can be determined by the boundary condition equations.

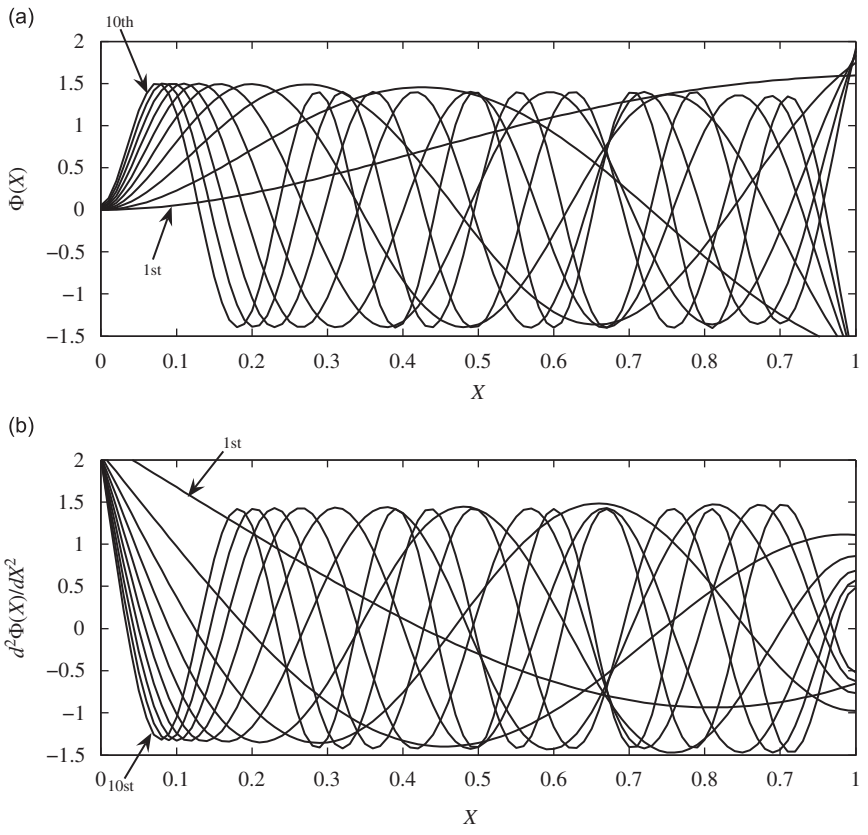

Fig. 6. (a) The first ten mode shapes and (b) the corresponding second spatial derivative of the mode shapes for Case A.

Rewriting the boundary condition equations in Eqs. (17) and (18) into dimensionless form, we obtain:

$$\frac{d^2\Phi(0)}{dX^2} - K_{L1}\frac{d\Phi(0)}{dX} = 0, \quad \frac{d^3\Phi(0)}{dX^3} + K_{L0}\Phi(0) = 0 \tag{30}$$

$$\frac{d^2\Phi(1)}{dX^2} + K_{R1}\frac{d\Phi(1)}{dX} = 0, \quad \frac{d^3\Phi(1)}{dX^3} - K_{R0}\Phi(1) = 0 \tag{31}$$

where $K_{L1} = k_{L1}L_x/EI$, $K_{L0} = k_{L0}L_x^3/EI$, $K_{R1} = k_{R1}L_x/EI$, $K_{R0} = k_{R0}L_x^3/EI$.

Substituting Eqs. (26)–(29) into Eqs. (30) and (31), we obtain:

$$\begin{bmatrix} 0 & -K_{L1} & 1 & 0 \\ K_{L0} & 0 & 0 & 1 \\ D_{31} & D_{32} & D_{33} & D_{34} \\ D_{41} & D_{42} & D_{43} & D_{44} \end{bmatrix} \begin{bmatrix} \Phi(0) \\ \frac{d\Phi(0)}{dX} \\ \frac{d^2\Phi(0)}{dX^2} \\ \frac{d^3\Phi(0)}{dX^3} \end{bmatrix} = 0 \tag{32}$$

where

$$D_{31} = \sum_{m=1}^{M-1}\left[\frac{k^m}{(4m-2)!} + K_{R1}\frac{k^m}{(4m-1)!}\right], \quad D_{32} = \sum_{m=1}^{M-1}\left[\frac{k^m}{(4m-1)!}\right] + K_{R1}\sum_{m=0}^{M-1}\left[\frac{k^m}{(4m)!}\right]$$

$$D_{33} = \sum_{m=0}^{M-1}\left[\frac{k^m}{(4m)!} + K_{R1}\frac{k^m}{(4m+1)!}\right], \quad D_{34} = \sum_{m=0}^{M-1}\left[\frac{k^m}{(4m+1)!} + K_{R1}\frac{k^m}{(4m+2)!}\right]$$

$$D_{41} = \sum_{m=1}^{M-1}\left[\frac{k^m}{(4m-3)!}\right] - K_{R0}\sum_{m=0}^{M-1}\left[\frac{k^m}{(4m)!}\right], \quad D_{42} = \sum_{m=1}^{M-1}\left[\frac{k^m}{(4m-2)!}\right] - K_{R0}\sum_{m=0}^{M-1}\left[\frac{k^m}{(4m+1)!}\right]$$

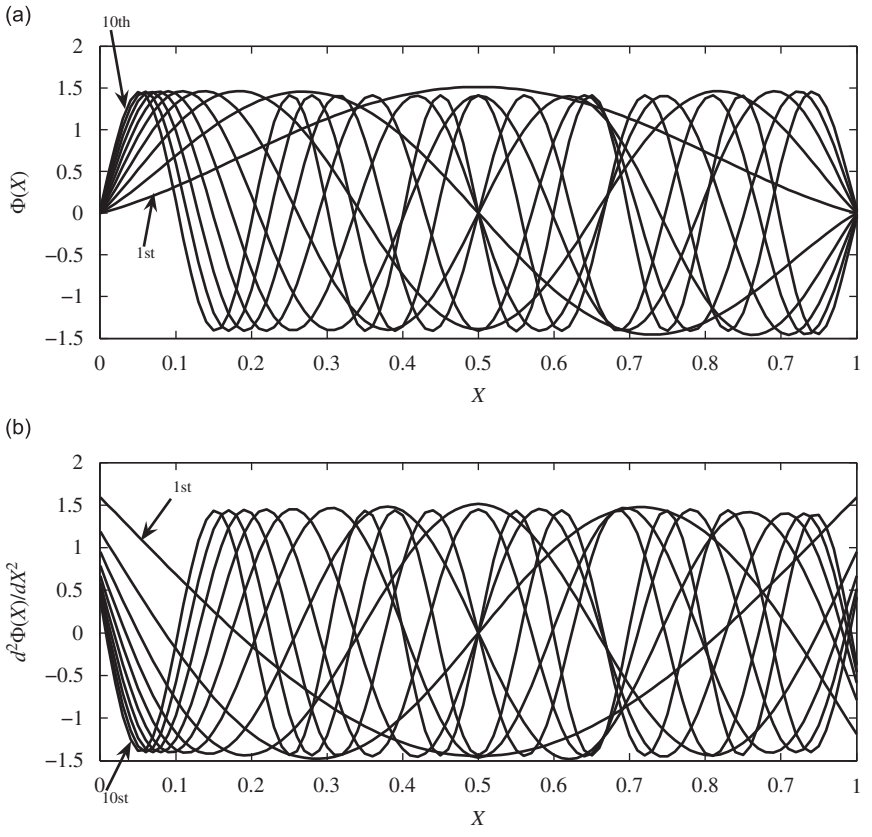

Fig. 7. (a) The first four mode shapes and (b) the corresponding second spatial derivative of the mode shapes for Case B.

$$D_{43}=\sum_{m=1}^{M-1}\left[\frac{k^m}{(4m-1)!}\right]-K_{R0}\sum_{m=0}^{M-1}\left[\frac{k^m}{(4m+2)!}\right],\quad D_{44}=\sum_{m=0}^{M-1}\left[\frac{k^m}{(4m)!}\right]-K_{R0}\sum_{m=0}^{M-1}\left[\frac{k^m}{(4m+3)!}\right]$$

From Eq. (32), the dimensionless frequency parameter k can be solved by

$$\det\begin{bmatrix}0 & -K_{RL} & 1 & 0\\ K_{TL} & 0 & 0 & 1\\ D_{31} & D_{32} & D_{33} & D_{34}\\ D_{41} & D_{42} & D_{43} & D_{44}\end{bmatrix}=0 \tag{33}$$

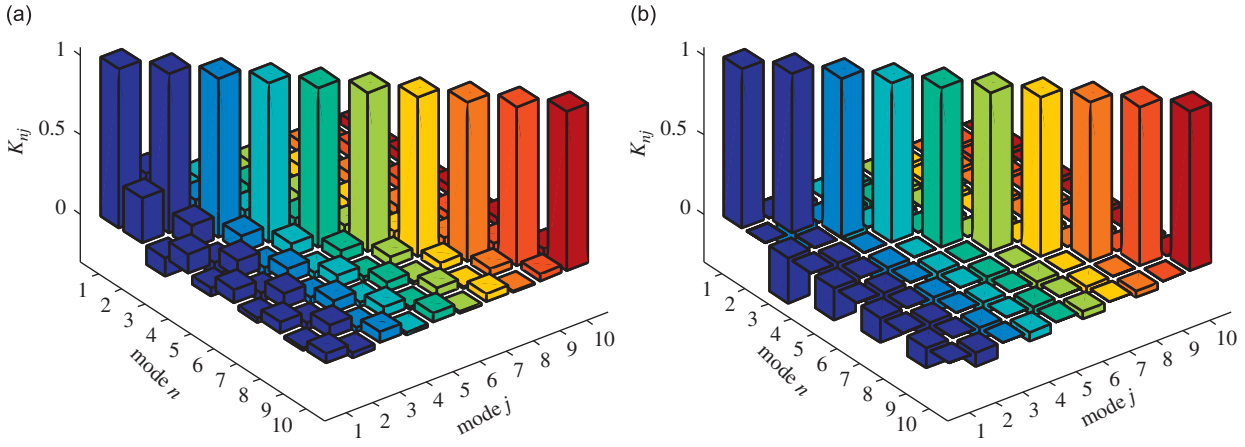

Fig. 8. Function K_{nj} in Eq. (8) for (a) Case A and (b) Case B.

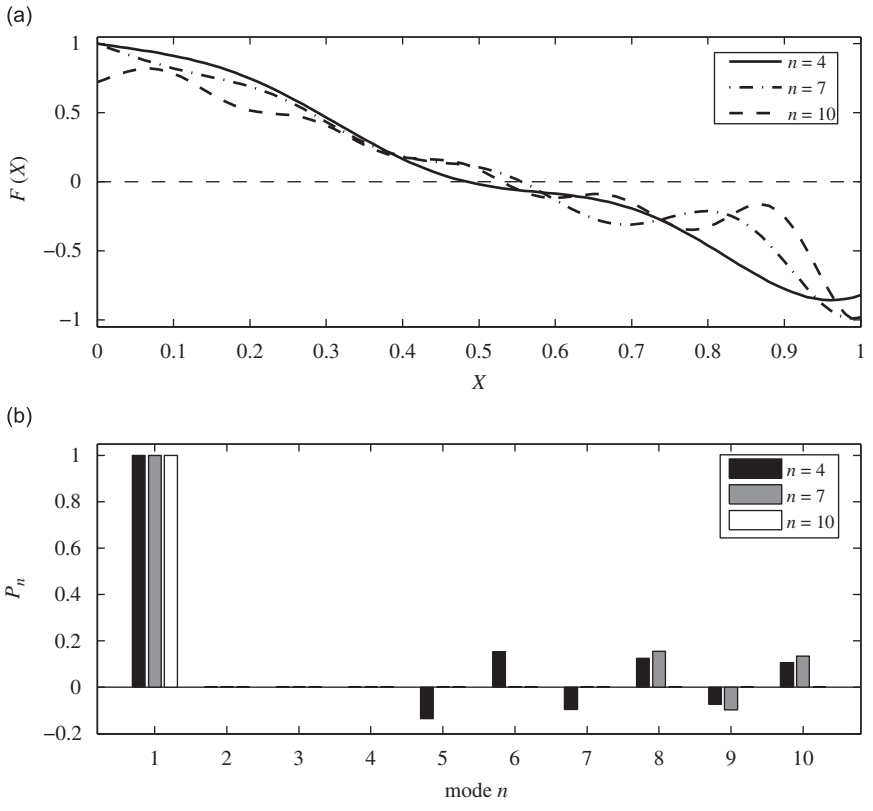

Fig. 9. The normalized PVDF shapes for the first modal sensors and corresponding normalized modal sensitivity P_n for Case A: (a) PVDF shapes and (b) modal sensitivity P_n.

Notice that the matrix in Eq. (32) is singular at each frequency parameter k, and the unknown parameters $d^n\Phi(0)/dX^n$ (n=0, 1, 2, 3) cannot be directly determined. However, one may choose one quantity of $d^n\Phi(0)/dX^n$ as the arbitrary nonzero constant, and the remaining three as functions of this arbitrary constant. Without loss of generality, one may choose $\Phi(0)=1$. Hence, the remaining three can be solved as functions by using Eq. (32):

$$\begin{bmatrix} 0 & 0 & 1 \\ D_{32} & D_{33} & D_{34} \\ D_{42} & D_{43} & D_{44} \end{bmatrix} \begin{bmatrix} \dfrac{d\Phi(0)}{dX} \\ \dfrac{d^2\Phi(0)}{dX^2} \\ \dfrac{d^3\Phi(0)}{dX^3} \end{bmatrix} = - \begin{bmatrix} K_{TL} \\ D_{31} \\ D_{41} \end{bmatrix} \tag{34}$$

By using Eqs. (34) and (28), the closed-form series solution for the second spatial derivative of the mode shapes $\partial^2\Phi(X)/\partial X^2$ can be obtained. It can be found that the solution of $\partial^2\Phi(X)/\partial X^2$ by using ADM is a continuous function and not discrete numerical values at knot point by finite element or finite difference methods.

Substituting $\partial^2\Phi(X)/\partial X^2$ into Eqs. (8) and (11), the PVDF sensor shape coefficients B_j are determined: Then substituting B_j into Eq. (5), the shape of the modal sensor can be obtained.

4. Numerical calculations

In order to verify the proposed method to design the PVDF modal sensor, the shapes of modal sensors with classical boundary conditions are first calculated and compared with analytical results in the literature [1,2,4]. The classical boundary conditions can be considered as special cases of Eq. (32). For example, the clamped boundary condition may basically be obtained by setting the stiffness of the linear and rotational springs to be extremely large. The stiffness of the translational and the rotational springs for the classical boundary conditions listed in Table 1 are used for the ADM calculations. The ADM solutions are truncated to M=20 in Eq. (26) throughout this paper.

According to the analysis in Section 2, for classical boundary conditions the shape of the modal sensor is proportional to the second spatial derivative of the mode shape of interest. Figs. 3–5 compare the shapes of the PVDF modal sensors for the first four structural modes by using the analytical method and the ADM for a clamped-free, simply supported and

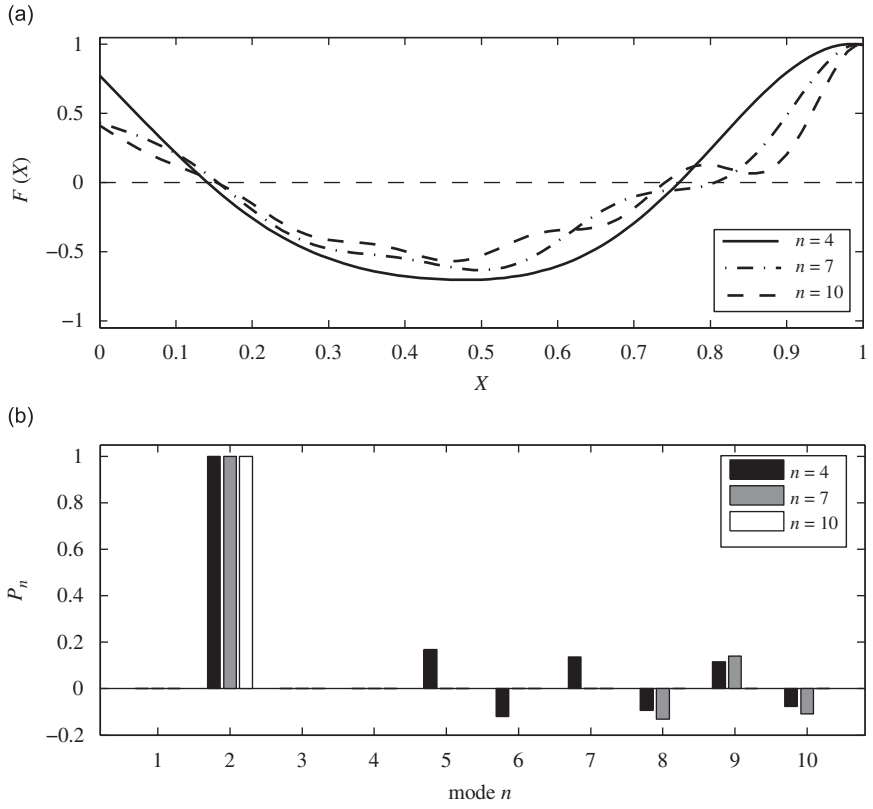

Fig. 10. The normalized PVDF shapes for the second modal sensors and corresponding normalized modal sensitivity P_n for Case A: (a) PVDF shapes and (b) modal sensitivity P_n.

clamped–clamped beam, respectively. The negative value of $F(X)$ means that the electric polarity of PVDF film is reversed. The sensor shapes can be observed as the mirror image of the corresponding mode shapes against the wall for the case of the clamped-free beam (See Fig. 3). For simply supported beam (See Fig. 4), the sensor shape is the same as the target structural mode shape. From Figs. 3–5, it can be shown that the PVDF sensor shapes designed by ADM are the same as the analytical results. This means that the design procedure using ADM has been successful.

In order to verify the ADM for general boundary conditions, two cases of general boundary conditions are discussed. The stiffness of the translational and the rotational springs for these two cases are listed in Table 2. Figs. 6 and 7 show the first ten mode shapes $\Phi(X)$ and the corresponding second spatial derivative of the mode shapes $\partial^2\Phi(X)/\partial X^2$ for both cases. Fig. 8 shows the function K_{nj} in Eq. (8) for Case A and B, respectively. From Fig. 8, it can be seen that the orthogonality of the second spatial derivative of the mode shapes cannot be satisfied for both cases. This is to be expected and implies that the modal sensor shape function $F(X)$ will not be proportional to the second spatial derivative of the mode shape of interest.

Figs. 9 and 10 show the normalized PVDF shapes for the first modal sensors and corresponding normalized modal sensitivity P_m as defined in Eq. (4) for Case A and Case B, respectively. From Figs. 9 and 10, it can be shown that the modal sensitivities $P_1=1$, and $P_n=0$ ($n=2$–N). This implies that by using ADM the modal sensors can filter out the responses of other involved modes, if for example, the first 4 modes involved for the design of modal sensor ($N=4$), P_n ($n=2, 3, 4$) are zero. Note that P_n ($n>4$) is not zero. This implies that this modal sensor may observe the responses of the $N > 4$ modes. This is to be expected since the designed sensor only considers the first 4 modes. If $N=10$ is used, the designed modal sensors can filter out the responses of the 2nd–10th modes. It should be noted that the PVDF shapes depend on the number of the modes of interest. If more modes involved, the sensor shapes are more complex. Figs. 11 and 12 show the normalized PVDF shapes for the second modal sensors and corresponding normalized modal sensitivity P_m for Cases A and B, respectively. It can be shown that the modal sensitivities $P_2=1$, and $P_n=0$ ($n=1$, 3–N).

To further demonstrate the performances of the sensors, an aluminum beam with dimensions of 500 mm × 40 mm × 5 mm is considered. The density and Young's modulus of the beam are 2700 Kg/m^3 and 7×10^{10} N/m^2, respectively. Assume that modal damping is 0.01. A point force located at $x_0 = L_x/10$ is used as the excitation. The first 10 natural frequencies calculated by ADM are listed in Table 3. Figs. 13 and 14 show the frequency response function (FRF) magnitudes of the modal sensors designed for the first and second modes for Cases A and B, respectively. The FRFs are the sensor current output $I(t) = \mathrm{d}Q(t)/\mathrm{d}t$ which are proportional to modal velocity $\mathrm{d}\eta(t)/\mathrm{d}t$. The FRFs are normalized at the natural frequency of the target mode. For low damping and well separated modes, the magnitude at a resonance peak is dominated by the

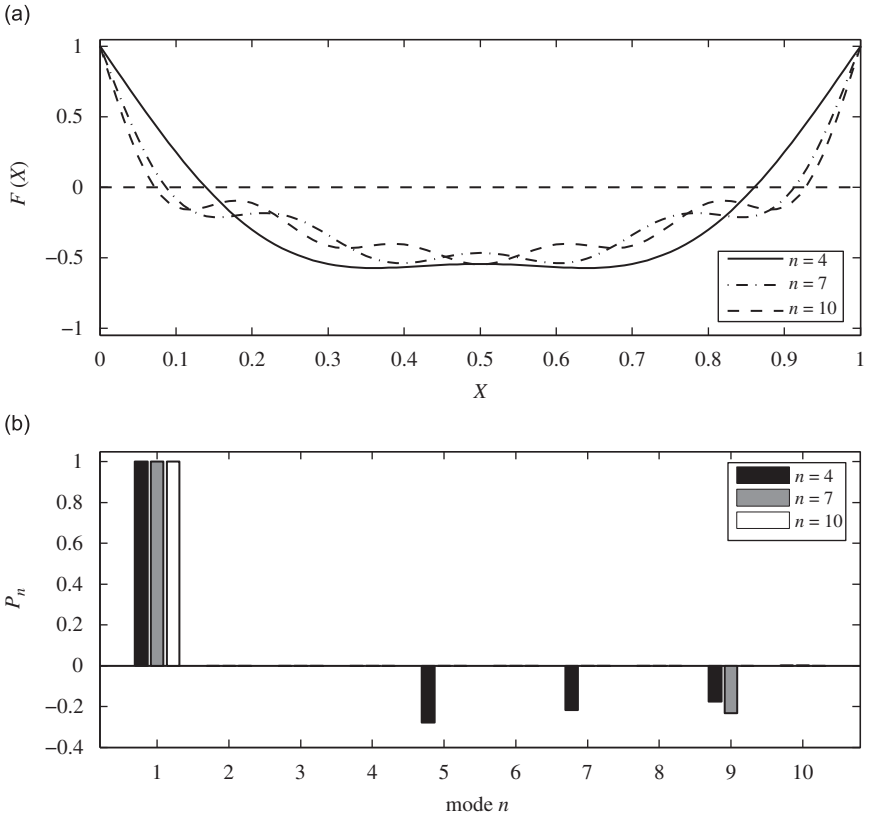

Fig. 11. The normalized PVDF shapes for the first modal sensors and corresponding normalized modal sensitivity P_n for Case B: (a) PVDF shapes and (b) modal sensitivity P_n.

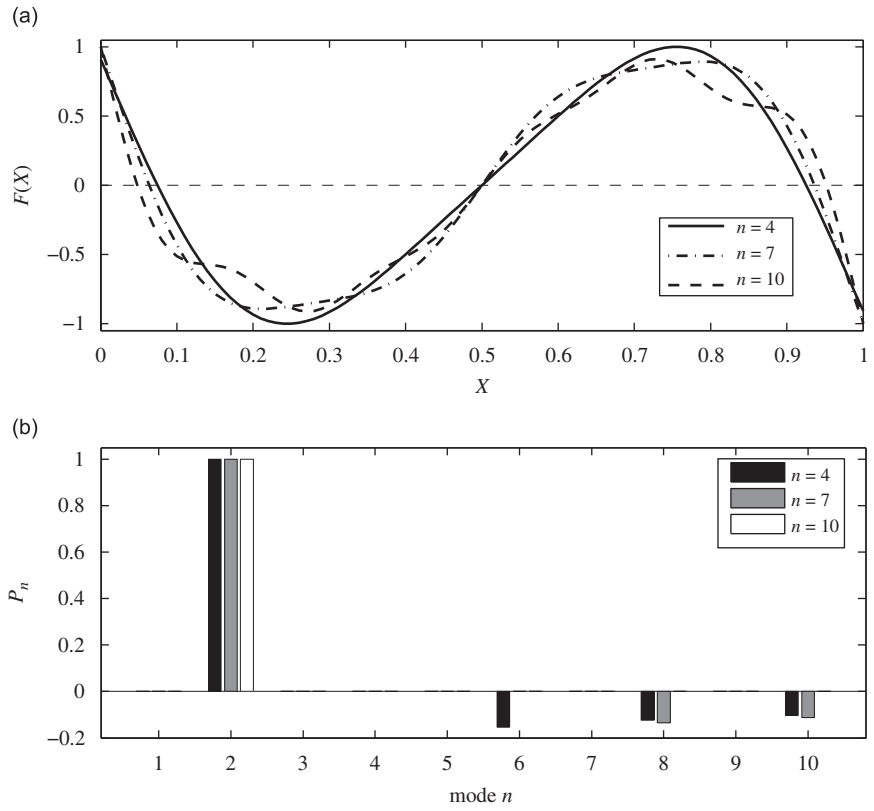

Fig. 12. The normalized PVDF shapes for the second modal sensors and corresponding normalized modal sensitivity P_n for Case B: (a) PVDF shapes and (b) modal sensitivity P_n.

Table 3
The first 10 natural frequencies for the beam with different boundary conditions (Hz).

Mode	1	2	3	4	5	6	7	8	9	10
Case A	46.2	184. 7	415.5	738.6	1153.9	1661.2	2260.5	2951.6	3734.3	4608.4
Case B	34.5	133.2	327.4	611.9	987.0	1452.9	2010.0	2658.3	3397.8	4228.2

contribution of the corresponding mode. The responses at the first and second natural frequencies dominate the FRFs in Figs. 13 and 14, respectively, as expected. The FRFs at high frequencies are strongly dependant on the shape of modal sensors and the modes involved. The proposed modal sensors can measure the target mode among the first N modes and filter out the rest of them. If N modes are involved in the design of modal sensor, no peak appears at the natural frequencies of those N modes except for the target mode. From Figs. 13 and 14, it can be shown that the modal sensor designed by N=10 modes can be considered to be a perfect modal filter in the frequency range 0–5000 Hz for both cases. It is concluded that for general boundary conditions the modal sensors can be considered to be modal filters in a limited frequency band.

5. Conclusions

A unified and systematic procedure is given to design shaped piezoelectric modal sensors for a beam with arbitrary boundary conditions by using the Adomian decomposition method (ADM). First, a general expression for designing the shape of piezoelectric modal sensor is presented based on the second spatial derivative of the mode shapes. Then the closed-form series solution for the second spatial derivative of the mode shapes is determined by using the ADM and performing some simple mathematical operations. The numerical results show that the PVDF modal sensor shapes designed by ADM are the same as the analytical results for the classical boundary conditions. This implies that the design procedure by using ADM has been successful, since for classical boundary conditions the shape of the modal sensor is proportional to the second spatial derivative of the mode shape of interest. Finally, two numerical examples of the beam with general boundary conditions are given. It is

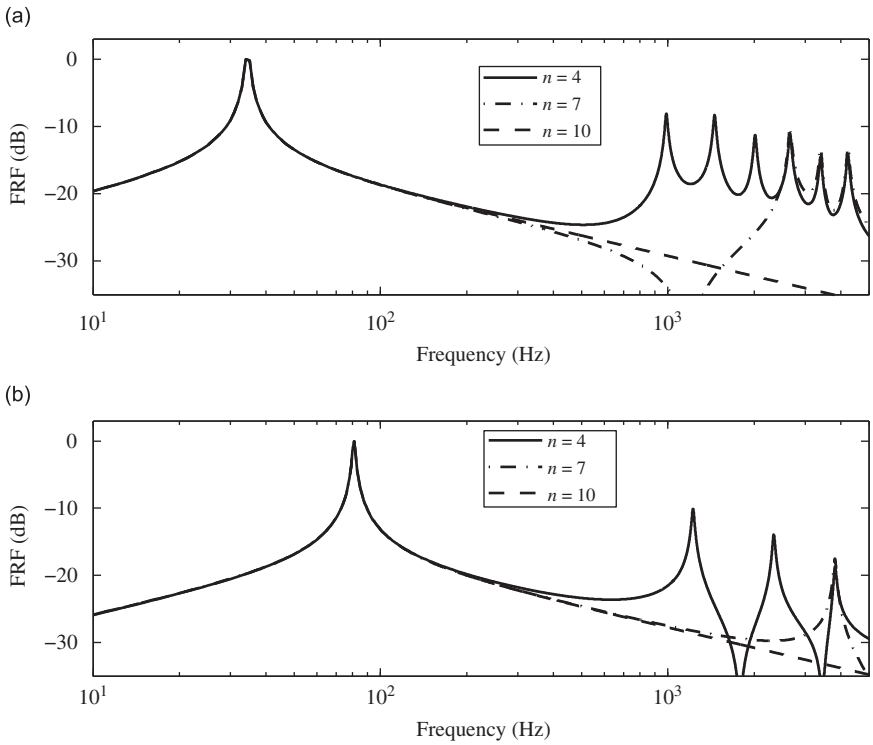

Fig. 13. The FRF magnitudes of the modal sensors designed for the first modes with unit amplitude at the first natural frequency for (a) Case A and (b) Case B.

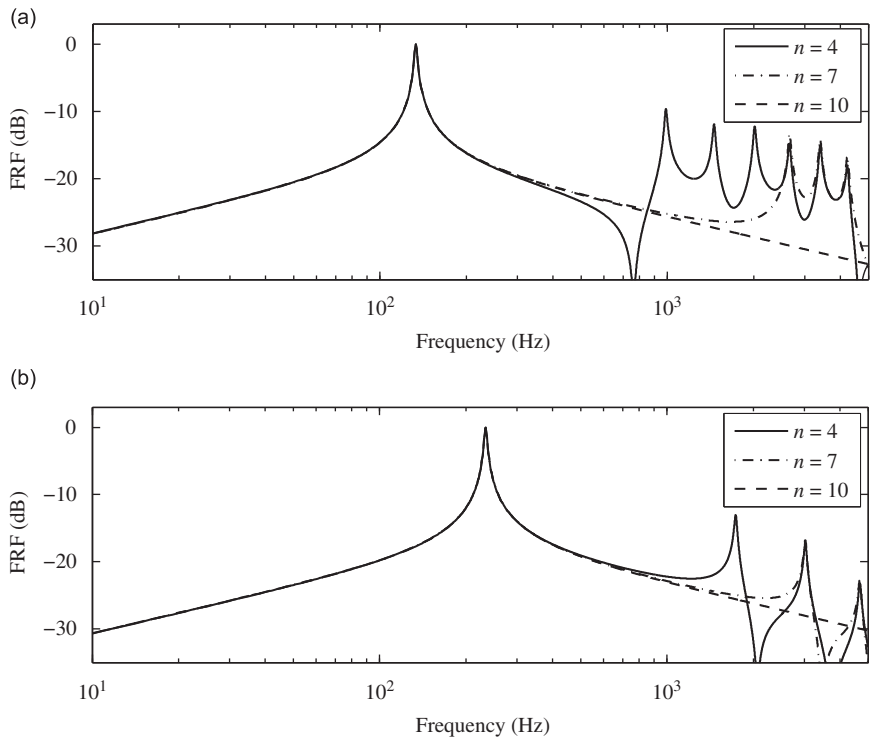

Fig. 14. The FRF magnitudes of the modal sensors designed for the second modes with unit amplitude at the second natural frequency for (a) Case A and (b) Case B.

shown that the modal sensors for general boundary conditions can be considered as modal filters within a limited frequency band. It should be noted that the proposed method for the design of modal sensors is universally applicable to arbitrary boundary conditions, including all classical cases. The design of modal sensors with different boundary conditions simply involves changing the value of stiffness of the translational and the rotational springs at the ends of the beam, and does not require any changes in the solution procedures or algorithms. However, the proposed method requires that the boundary conditions or the second spatial derivative of mode shapes $\partial^2\Phi(X)/\partial X^2$ should be known accurately. Theoretical and experimental modal analysis technique based on PVDF sensor to directly obtain $\partial^2\Phi(X)/\partial X^2$, proposed by Ref. [30], will be the subject of further research.

Appendix A. A brief review of Adomian decomposition method (ADM)

In this appendix, the concept of Adomian decomposition method (ADM) is briefly introduced. Consider the general nonlinear functional equation:

$$Lu(x)+Ru(x)+Nu(x)=g(x) \tag{A.1}$$

where L is a linear invertible operator of highest-order derivative with respect to x. R is the remainder linear operator. N is the nonlinear operator, and $g(x)$ is the source term.

As L is invertible, Eq. (A.1) can be rewritten as

$$L^{-1}Lu(x)=L^{-1}g(x)-L^{-1}Ru(x)-L^{-1}Nu(x) \tag{A.2}$$

where L^{-1} can be an integral operator defined from 0 to x.

Assume that $L=\mathrm{d}^4/\mathrm{d}x^4$, we will have:

$$L^{-1}=\int_0^x\int_0^x\int_0^x\int_0^x(\ldots)\,\mathrm{d}x\,\mathrm{d}x\,\mathrm{d}x\,\mathrm{d}x \tag{A.3}$$

and

$$L^{-1}Lu(x)=u(x)-u(0)-x\frac{\mathrm{d}u(0)}{\mathrm{d}x}-\frac{x^2}{2}\frac{\mathrm{d}^2u(0)}{\mathrm{d}x^2}-\frac{x^3}{6}\frac{\mathrm{d}^3u(0)}{\mathrm{d}x^3} \tag{A.4}$$

Comparing Eq. (A.4) and (A.2), we obtain:

$$u(x)=u(0)+x\frac{\mathrm{d}u(0)}{\mathrm{d}x}+\frac{x^2}{2}\frac{\mathrm{d}^2u(0)}{\mathrm{d}x^2}+\frac{x^3}{6}\frac{\mathrm{d}^3u(0)}{\mathrm{d}x^3}+L^{-1}g(x)-L^{-1}Ru(x)-L^{-1}Nu(x) \tag{A.5}$$

According to the standard Adomian decomposition method [23–25], it defines the solution $u(x)$ by an infinite series of the form:

$$u(x)=\sum_{m=0}^{\infty}u_m(x) \tag{A.6}$$

And for the nonlinear term $Nu(x)$, it defines:

$$Nu(x)=\sum_{m=0}^{\infty}A_m(x) \tag{A.7}$$

where the A_m are called Adomian's polynomials [24,25].

Substituting Eqs. (A.6) and (A.7) into Eq. (A.5), we obtain:

$$\sum_{m=0}^{\infty}u_m(x)=u_0(x)-L^{-1}R\sum_{m=0}^{\infty}u_m(x)-L^{-1}\sum_{m=0}^{\infty}A_m(x) \tag{A.8}$$

where $u_0(x)$ is defined as

$$u_0(x)=u(0)+x\frac{\mathrm{d}u(0)}{\mathrm{d}x}+\frac{x^2}{2}\frac{\mathrm{d}^2u(0)}{\mathrm{d}x^2}+\frac{x^3}{6}\frac{\mathrm{d}^3u(0)}{\mathrm{d}x^3}+L^{-1}g(x) \tag{A.9}$$

Finally, each term $u_m(x)$ in Eq. (A.8) is deduced by the following recurrence relation:

$$\begin{cases} u_1(x)=-L^{-1}Ru_0(x)-L^{-1}A_0(x)\\ u_2(x)=-L^{-1}Ru_1(x)-L^{-1}A_1(x)\\ \vdots\\ u_{m+1}(x)=-L^{-1}Ru_m(x)-L^{-1}A_m(x)\end{cases} \tag{A.10}$$

Substituting Eqs. (A.9) and (A.10) into Eq. (A.6), we can obtain the solution of $u(x)$ if the series in Eq. (A.10) converges. The convergence of ADM is proved by Refs. [31,32].

References

[1] C.K. Lee, F.C. Moon, Modal sensors/actuator, *Journal of Applied Mechanics* 57 (1990) 434–441.
[2] N. Tanaka, S.D. Snyder, C.H. Hansen, Distributed parameter modal filtering using smart sensors, *ASME Transactions on Journal of Vibration and Acoustics* 118 (1996) 630–640.
[3] N. Tanaka, T. Sanada, Modal control of a rectangular plate using smart sensors and smart actuators, *Smart Materials and Structures* 16 (2007) 36–46.
[4] W. Gawronski, Modal actuators and sensors, *Journal of Sound and Vibration* 229 (2000) 1013–1022.
[5] D.K. Anthony, Modal detection for non-uniform thickness beams using continuous strain sensors and a strain-energy-based orthogonality condition, *Journal of Sound and Vibration* 315 (2008) 65–87.
[6] A. Donoso, J.C. Bellido, Distributed piezoelectric modal sensors for circular plates, *Journal of Sound and Vibration* 319 (2009) 50–57.
[7] R.L. Clark, S.E. Burke, Practical limitations in achieving shaped modal sensors with induced strain materials, *ASME Transactions on Journal of Vibration and Acoustics* 118 (1996) 668–675.
[8] K. Jian, M.I. Friswell, Distributed modal sensors for rectangular plate structures, *Journal of Intelligent Material Systems and Structures* (2007) 939–948.
[9] B.Z. Marcellin, K. Naghshineh, J.W. Kamman, Narrow band active control of sound radiated from a baffled beam using local volume displacement minimization, *Applied Acoustics* 62 (2001) 47–64.
[10] F. Charette, A. Berry, C. Guigou, Active control of sound radiation from a plate using a polyvinylidence fluoride volume displacement sensor, *Journal of the Acoustical Society of America* 103 (3) (1998) 1493–1503.
[11] S.D. Snyder, N. Tanaka, Y. Kikushima, The use of optimally shaped piezo-electric film sensors in the active control of free field structural radiation, part 1: feedforward control, *ASME Transactions on Journal of Vibration and Acoustics* 117 (1995) 311–322.
[12] B.S. Cazzolato, C.H. Hansen, Structural radiation mode sensing for active control of sound radiation into enclosed spaces, *Journal of the Acoustical Society of America* 106 (6) (1999) 3732–3735.
[13] P. Gardonio, Y.S. Lee, S.J. Elliott, Analysis and measurement of a matched volume velocity sensor and uniform force actuator for active structural acoustic control, *Journal of the Acoustical Society of America* 110 (6) (2001) 3025–3031.
[14] H. Henrioulle, P. Sas, Experimental validation of a collocated PVDF volume velocity sensor/actuator pair, *Journal of Sound and Vibration* 265 (2003) 489–506.
[15] Q. Mao, B. Xu, Z. Jiang, J. Gu, A piezoelectric array for sensing radiation modes, *Applied Acoustics* 64 (2003) 669–680.
[16] Q. Mao, S.J. Pietrzko, Measurements of local volume displacement using a piezoelectric array, *Acta Acustica United with Acustica* 92 (2006) 556–566.
[17] A. Preumont, A. Francois, P.D. Man, V. Piefort, Spatial filters in structural control, *Journal of Sound and Vibration* 265 (2003) 61–79.
[18] A. Preumont, A. Francois, P.D. Man, N. Loix, K. Henrioulle, Distributed sensors with piezoelectric films in design of spatial filters for structural control, *Journal of Sound and Vibration* 283 (2005) 701–712.
[19] B.Z. Marcellin, J.W. Kamman, K. Naghshineh, Theoretical development and experimental validation of local volume displacement sensors for a vibrating beam, *ASME Transactions on Journal of Vibration and Acoustics* 123 (2001) 110–118.
[20] S. Sivrioglu, N. Tanaka, I. Yuksek, Acoustic power suppression of a panel structure using h_∞ output feedback control, *Journal of Sound and Vibration* 249 (2002) 885–897.
[21] M.I. Friswell, On the design of modal actuators and sensor, *Journal of Sound and Vibration* 241 (2001) 361–372.
[22] K. Jiana, M.I. Friswell, Designing distributed modal sensors for plate structures using finite element analysis, *Mechanical Systems and Signal Processing* 20 (2006) 2290–2304.
[23] G. Adomian, *Solving Frontier Problems of Physics: The Decomposition Method*, Kluwer-Academic Publishers, Boston, MA, 1994.
[24] M. Javidi, A. Golbabai, Adomian decomposition method for approximating the solution of the parabolic equations, *Applied Mathematical Sciences* 1 (5) (2007) 219–225.
[25] A.M. Wazwaz, Analytic treatment for variable coefficient fourth-order parabolic partial differential equations, *Applied Mathematics and Computation* 123 (2001) 219–227.
[26] H. Haddadpour, An exact solution for variable coefficients fourth-order wave equation using the Adomian method, *Mathematical and Computer Modelling* 44 (2006) 1144–1152.
[27] H.-Y. Lai, J.-C. Hsu, C.K. Chen, An innovative eigenvalue problem solver for free vibration of Euler–Bernoulli beam by using the Adomian decomposition method, *Computers and Mathematics with Applications* 56 (12) (2008) 3204–3220.
[28] J.-C. Hsu, H.-Y. Lai, C.K. Chen, Free vibration of non-uniform Euler–Bernoulli beams with general elastically end constraints using Adomian modified decomposition method, *Journal of Sound and Vibration* 318 (2008) 965–981.
[29] S. Das, A numerical solution of the vibration equation using modified decomposition method, *Journal of Sound and Vibration* 320 (3) (2008) 576–583.
[30] R.-L. Chen, C.-C. Wang, The use of polyvinylidene fluoride films as sensors for the experimental modal analysis of structures, *Smart Materials and Structures* 13 (2004) 791–799.
[31] K. Abbaoui, Y. Cherruault, Convergence of Adomian's method applied to nonlinear equations, *Mathematical and Computer Modelling* 20 (9) (1994) 69–73.
[32] Y. Cherruault, G. Adomian, K. Abbaoui, R. Rach, Further remarks on convergence of decomposition method, *International Journal of Bio-Medical Computing* 38 (1) (1995) 89–93.